Memoirs of the Faculty of Science, Kyoto University, Series of Physics, Astrophysics, Geophysics and Chemistry, Vol. XXXV, No. 1, Arteicle 2, 1977.

PHOTOPRODUCTION OF NEUTRAL PIONS OFF DEUTERIUM IN THE ENERGY REGION BETWEEN 300 MeV AND 700 MeV

BY

Nobuyuki YAMASHITA

Department of Physics, Kyoto University, Kyoto

(Received October 16, 1974)

ABSTRACT

The ratios of the differential cross sections, $R=[d\sigma/d\Omega(\gamma+n\to\pi^\circ+n)]/[d\sigma/d\Omega(\gamma+p\to\pi^\circ+p)]$ have been measured at the four pion c.m. angles of 70°, 90°, 110° and 130° in the energy region between 300 MeV and 700 MeV. Two photons decayed from the π° meson and the recoil nucleon have been detected in coincidence. The results are analyzed basing on the recent phenomenological partial wave analysis. The isotensor amplitude is estimated to be less than 3% of the isovector amplitude at the first resonance. In the region of the second resonance the results are consistent with the recent phenomenological analyses. There is no enhancement of the cross section for the reaction $\gamma+n\to\pi^\circ+n$ due to the $N(1470)$ (P_{11}) resonance.

I. Introduction

In recent years the experiments on the signle pion photoproduction in the resonance region have been performed extensively. The experimental results have been analyzed phenomenologically in terms of the resonance amplitudes. These results were compared with the theoretical prediction from such as the quark model. However, the experimental results for the single pion photoproduction are still not so abundant and precise as compared to those of, for example, the $\pi-N$ interactions.

In terms of isospin amplitudes, the amplitudes of pion photoproduction are decomposed as follows[1,10];

$$3A(\gamma p\to\pi^\circ p)=3A^0+A^1+2A^3-2\sqrt{3/5}A^2\,, \tag{1-1a}$$

$$3A(\gamma n\to\pi^\circ n)=3A^0+A^1+2A^3+2\sqrt{3/5}A^2\,, \tag{1-1b}$$

$$3/\sqrt{2}\,A(\gamma p\to\pi^+ n)=3A^0+A^1-A^3+\sqrt{3/5}A^2\,, \tag{1-1c}$$

$$3/\sqrt{2}\,A(\gamma n\to\pi^- p)=3A^0-A^1+A^3+\sqrt{3/5}A^2\,, \tag{1-1d}$$

where A^0 and A^1 are the isoscalar and isovector amplitudes leading to the final πN states with $I=1/2$, respectively. A^3 and A^2 are the isovector and isotensor amplitudes, leading to the final states with $I=3/2$ respectively. In order to investigate the behaviour of the resonance amplitudes in the isospin space, the informations on the photoproduction off nuetrons are necessary as well as those for protons. The experimental results of neutron target were not abundant because of

the difficulty of the experiment by using the deuterium target. However, recently a few experiments[4),5),7),8),9),11),25)] by using the deuterium target have been performed to study the details of the amplitudes in the isospin space.

The possibility of the existence of the isotensor current, which are represented by the forth terms in equation (1-1), was firstly suggested in Ref. 2. Sanda and Shaw[3)] analyzed the experimental results to estimate the contribution of this current in photo-excitation of the $\Delta(1236)$ resonance, which is known as 'the dip test'. They evaluated the difference between the total cross sections of the reactions (1-1d) and (1-1c) in the energy region of the $\Delta(1236)$ resonance;

$$\Delta'(W)=k^c/q^c[\sigma_t(\gamma n\rightarrow\pi^- p)-\sigma_t(\gamma p\rightarrow\pi^+ n)]\,, \qquad (1\text{-}2)$$

where σ_t represents the total cross section of each reaction. W, k^c and q^c represent the total energy, photon and pion momentum in the c.m. system, respectively.

If there is the isotensor current term in the amplitude of the first resonance, $\Delta'(W)$ will exhibit the dip or bump behaviour because the sign of A^2 is opposite each other for neutron and proton targets. In fact, according to the analysis by Sanda and Shaw, the results of the earlier bubble chamber experiments[4,5)] for the reaction $\gamma+n\rightarrow\pi^-+p$ showed the dip structure in $\Delta'(W)$ as is shown in Fig. 1. Then they concluded that the contribution of the isotensor current to the photo-excitation of the $\Delta(1236)$ resonance amounted to be 20–30 % in the amplitude. The result of the inverse reaction $\pi^-+p\rightarrow\gamma+n$[6)] also supported their conclusion.

Recently, ABHHM[7)] reanalyzed their data in detail with the deuteron correction. Also recently counter experiments for the reactions (1-1c), (1-1d) have been performed at INS[8)] and Bonn[9)]. In these counter experiments, the positive and negative pions off deuterons were detected with the same apparatus. Therefore, the ratio π^-/π^+ thus measured is expected to be almost free from the deuteron corrections. According to these results the dip of $\Delta'(W)$ disappeared.

The dip of the difference $\Delta'(W)$, which was exhibited first by Sanda and Shaw,

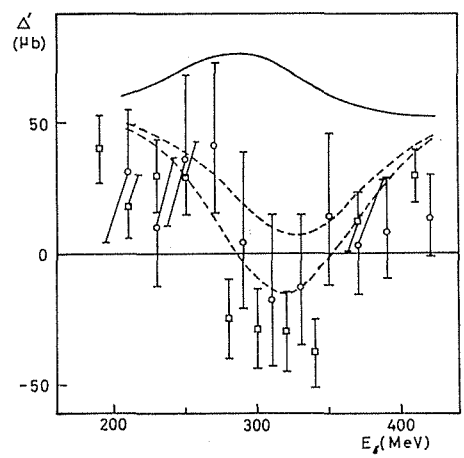

Fig. 1. Dip test of the difference of the total cross sections of the equation (1-2) given by Sanda and Shaw. The open circles and open squares represent the results of Ref. 4 and Ref. 5, respectively.

was not so large and about 1/6 of the total cross section $\sigma_t(\gamma+n\to\pi^-+p)$ or $\sigma_t(\gamma+p\to\pi^++n)$. Moreover, the extraction of the cross section for neurtrons from the experiment using the deuterium target is not straightforward.

On the other hand, the experiment for the reaction $\gamma+n\to\pi^\circ+n$ is very sensitive to test the existence of the isotensor current, because in this reaction the electric Born terms vanish and the resonance amplitude is dominant. Furthermore, as is seen from equations (1−1a)−(1−1d), for the π° production the I=3/2 terms are enhanced relative to the I=1/2 terms compared to the charged pion production. Then if the amplitude of the $\Delta(1236)$ resonance for the neutron target decreases to 0.7 of that for the proton target due to the isotensor term, the total cross section of the reaction $\gamma+n\to\pi^\circ+n$ at 340 MeV is expected to be 0.51[10] times smaller than that of the case without the isotensor term. The differential cross sections are also expected to decrease by about the same amount, because that the $\Delta(1236)$ ampiltude is dominant in this energy region.

The experimental informations on the reaction $\gamma+n\to\pi^\circ+n$ at higher energies are also useful to determine the isoscalar amplitude. In the second resonance region, the I=1/2 resonances such as $N(1470)$ (P_{11}), $N(1535)$ (S_{11}) and $N(1520)$ (D_{13}) play an important role. These I=1/2 resonances can be photo-excited through the isovector and isoscalar amplitudes. Although there have been a few experiments[11),25)] in this energy region, more experimental informations are needed.

In order to clarify the contribution of the isotensor current at the $\Delta(1236)$ resonance region, and to obtain further informations on the isoscalar current at the second resonance region, we have measured the differential cross section of the reactions $\gamma+n\to\pi^\circ+n$ and $\gamma+p\to\pi^\circ+p$ by using the deuterium target at the same time in the photon energy region from 300 MeV to 700 MeV and at the c.m. angles of 70°, 90°, 110° and 130°.

The experiment has been performed by detecting both of decayed photons from the π° meson and the recoil nucleon in coincidence. The details of the detection system are described in section II.

The results on the ratio $R=[d\sigma/d\Omega(\gamma+n\to\pi^\circ+n)]/[d\sigma/d\Omega(\gamma+p\to\pi^\circ+p)]$ are described and discussed in section V.

II. Experimental equipments

II-1 General description

The bremsstrahlung beam from the 1.3 GeV electron synchrotron at the Institute for Nuclear Study, University of Tokyo, was incident on the liquid deuterium target. The four momentum vectors of both the π° meson and the recoil nucleon were measured, since the target nucleon is moving in the deuteron. The schematic layout of the experimental apparatus is presented in Fig. 2. The basic detection system is similar to that of Ref. 11. However some improvements were made on the π° detector. The π° meson was detected with a pair of γ detectors. The recoil nucleon was detected with a plastic scintillation hodoscope and with thin plastic scintillators which was set in front of the hodoscope to identify the charge of the nucleon. The momentum of the nucleon was measured with the time of flight method (TOF).

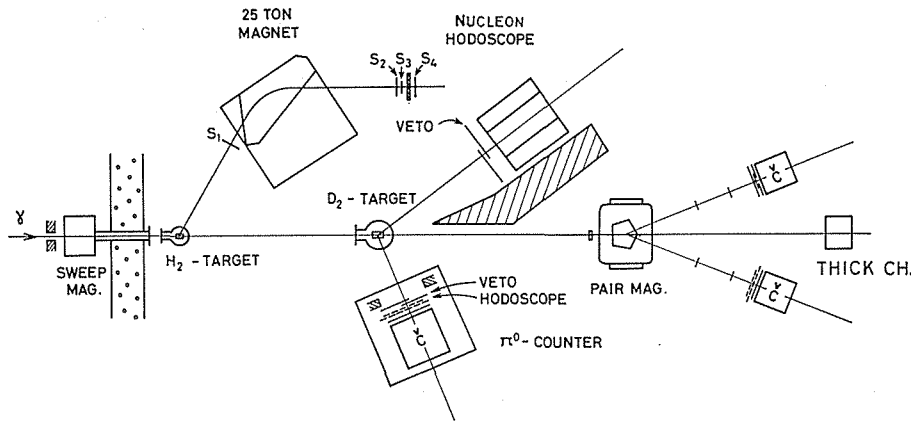

Fig. 2. Schematic layout of the apparatus. The calibration systems for the nucleon hodoscope and the γ detector are also shown.

II-2 Beam and target

The bremsstrahlung beam produced at the platinum radiator of 50 μm in thickness in the synchrotron was shaped by a double collimation system. The beam was collimated with the first lead collimator of 5 mm in diameter, and passed through a sweep magnet. A halo around the beam was removed with the second collimator of 12 mm in diameter. Another sweep magnet was set at the down stream of the second collimator. The profile of the beam was 25 mm in diameter at the target position.

The container of liquid deuterium or hydrogen was a cylindrical shape of 10.8 cm in length along the beam axis and 4 cm in diameter, and was made of Mylar.

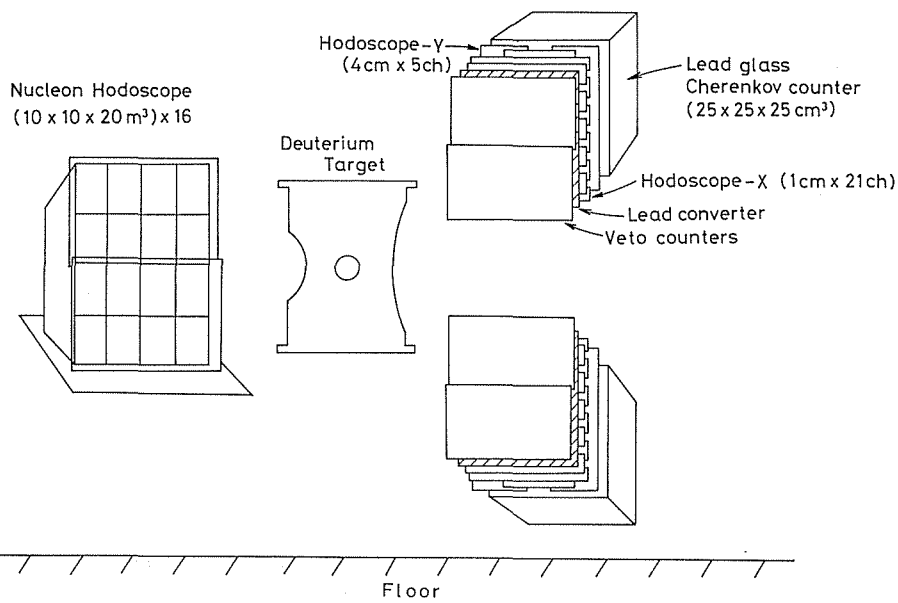

Fig. 3. Experimental setup viewed from the up-stream of the bremsstrahlung beam.

The thickness of the side wall of the container was 125 μm and that of the beam windows was 75 μm. A vacuum chamber had Mylar windows of 250 μm in thickness. Especially in the direction of the photons decayed from the π° meson, the window was large enough to pass the photon from the π° meson having an opening angle of $\pm 41^\circ$ with respect to the horizontal plane, as is shown in Fig. 3. This target system utilizes a small mechanical refrigerator[12] to liquify the gas and to maintain it in the target container.

The intensity of the bremsstrahlung beam was monitored with a thick-walled ionization chamber throughout the experiment.

II-3 π° detection

Both of two photons decayed from the π° meson were detected with a pair of γ detectors. Each γ detector consisted of a LiH hardener, a veto counter, a lead converter of 5.0 mm in thickness, an x-y plastic scintillation hodoscope and a lead glass Cherenkov counter of total absorption type. These γ detectors were set symmetrically about the horizontal plane to get a good angular resolution for the π° meson. The π° detector was set on a rotatable platform. Each γ detector was drived up- and downwards by a motor. The opening angle between two γ detectors, Ψ, was set to be equal to the minimum correlation angle (*i.e.* the angle of symmetrical decay) depending on the π° energy. The minimum correlation angle is defined as follows;

$$\sin\frac{\Psi}{2}=\frac{\mu}{\omega_\pi}, \tag{2-1}$$

where μ and ω_π represent the mass and the energy of the π° meson, respectively.

a) Cherenkov counter[13]

The total absorption Cherenkov counter was made of SF-2 lead glass of 25 cm cube (8.8 radiation lengths). In the present experiment, it was necessary to detect low energy photons of 50 MeV. The number of photomultipliers (RCA 6655A), which were optically contacted with the lead glass by silicon rubber, was originally 9 in the previous experiment and increased to 16 for this experiment. The thickness of the lead converter was decreased to about 1 radiation length from 2 radiation lengths. The linearity and energy resolution of the Cherenkov counters were measured with the electron beam which was analyzed by a magnet, as is shown in Fig. 2. The results are shown in Fig, 4. The energy dependence of the resolution was found to be expressed by

$$\Delta E_\gamma/E_\gamma=4.58/\sqrt{E_\gamma-30.0}\quad(\text{FWHM}), \tag{2-2}$$

where E_γ denotes the energy of the incident photon in the unit of MeV.

b) x-y hodoscope and the veto counter

The photons decayed from the π° meson were converted to electrons and positrons by the lead converters. Then the incident positions of the photons were observed by the scintillation hodoscope which was set behind the lead converter, The hodoscope limitted the area of the incident position within 20×21 cm^2 to eliminate the events occured at the edge of the lead glass. As is shown in Fig. 3, the hodoscope consisted of two layers of Pilot Y scintillators of 1/4 inch in thickness.

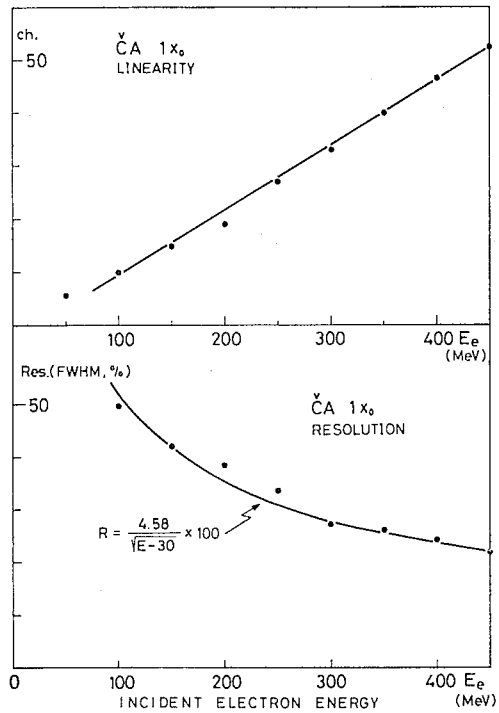

Fig. 4. Linearity and energy resolution of the Cherenkov counter for monochromatic electrons using a lead converter of 5 mm in thickness.

The vertical hodoscope (x) was made of 11 counters viewed by XP 1110 photomultipliers, which was mounted to overlap so as to provide 21 bins of 1 cm in width and 20 cm in height. The horizontal hodoscope (y) was made of 3 counters viewed by RCA 6655A photomultipliers to provide 5 bins of 4 cm in width and 21 cm in height.

The veto counters consisted of a pair of Pilot Y scintillators of 1/4 inch in thickness viewed by RCA 6655A photomultipliers.

Lithium hydride (LiH) absorbers were placed in front of the veto counters to absorb low energy photons. The thickness of this absorber was 0.1–0.2 radiation lengths.

II-4 Nucleon detection

a) Nucleon hodoscope

We detected protons and neutrons at the same time with a plastic scintillation hodoscope consisting of 16 modules, each of which had an aperture of 10×10 cm^2 and a length of 20 cm and viewed by an RCA 6655A photomultiplier through a Lucite light guide. The gain of each module was calibrated by the proton at a few energies by using the magnetic analyzer system as is shown in Fig. 2. The proton was separated from the π^+ meson by dE/dx in S1-S4 counters and by TOF between S1 and S3 counters.

By using the hydrogen target, the detection efficiency of the nucleon hodoscope for neutrons was measured by detecting the recoil neutron from the reaction

$\gamma+p\rightarrow\pi^{+}+n$. In order to determine the kinetic energy of the neutrons the four momentum vectors of π^{+} mesons were measured by using the magnetic analyzer system used in the proton detection Fig. 2. The proton was rejected by an absorber and TOF between S1 and S3 counters. Then the detection efficiency for the neutron, η_n, was obtained by the following coincidence ratio;

$$\eta_n=\frac{N(n\cdot\pi^{+})}{g\cdot N(\pi^{+})}, \tag{2-3}$$

where $N(\pi^{+})$ represents the yield of the π^{+} meson and $N(n\cdot\pi^{+})$ represents the number of the coincidence between the π^{+} meson and the neutron. The parameter g represents the geometrical detection efficiency for the neutron tagged by the π^{+} meson and was calculated to be 1.00–0.97 by a Monte Carlo simulation. The results of the detection efficiency in the kinetic energy region between 30 MeV and 200 MeV for three bias sets are shown in Fig. 5. The measurement of reaction $\gamma+n\rightarrow\pi^{\circ}+n$ has been performed with 10 and 15 MeV bias sets.

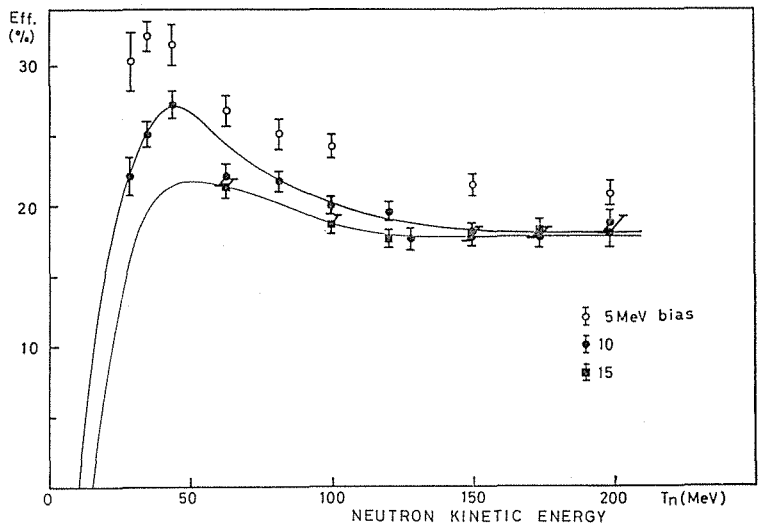

Fig. 5. Detection efficiencies of the nucleon hodoscope for neutrons versus the neutron kinetic energy. The measured values for three cases in which the bias of the nucleon hodoscope was set at 5 MeV, 10 MeV and 15 MeV in terms of the proton kinetic energy are indicated with the open circles, closed circles and closed squares, respectively.

b) Thin plastic scintillator

In front of the nucleon hodoscope a pair of thin plastic scintillation counters were set to distinguish between the proton and the neutron. Each counter was made of 3 mm thick Pilot *Y* scintillator having the dimension of 21 cm×42 cm and viewed by 56 AVP photomultipliers from both ends.

The inefficiency of these counters for the proton plays an important role to determine the ratio $R=[d\sigma/d\Omega(\gamma+n\rightarrow\pi^{\circ}+n)]/[d\sigma/d\Omega(\gamma+p\rightarrow\pi^{\circ}+p)]$. The inefficiency was evaluated by two different ways. At first the inefficiency was measured by detecting momentum analyzed protons with the same system as described

in sub-section IV-2-a). Secondly when the coincidence was occured between the nucleon hodoscope and the π° detector in the hydrogen target run, the inefficiency was reduced from the false events rate in which the proton was recorded as the neutron. The inefficiency thus evaluated was

$$\eta_{\text{ineff.}} = 0.45 \pm 0.04\% ,$$

and was taken into the data reduction.

In data taking runs in which the nucleon hodoscope was placed close to the photon beam, a lead absorber of 1-6 mm in thickness was set to reduce the low energy background.

The momentum of the nucleon was obtained from TOF by using the photon signal from one of the γ detectors as the start pulse and the nucleon signal as the stop pulse. The TOF resolution of 1 ns (FWHM) was achieved by utilizing the pulse height compensation method.

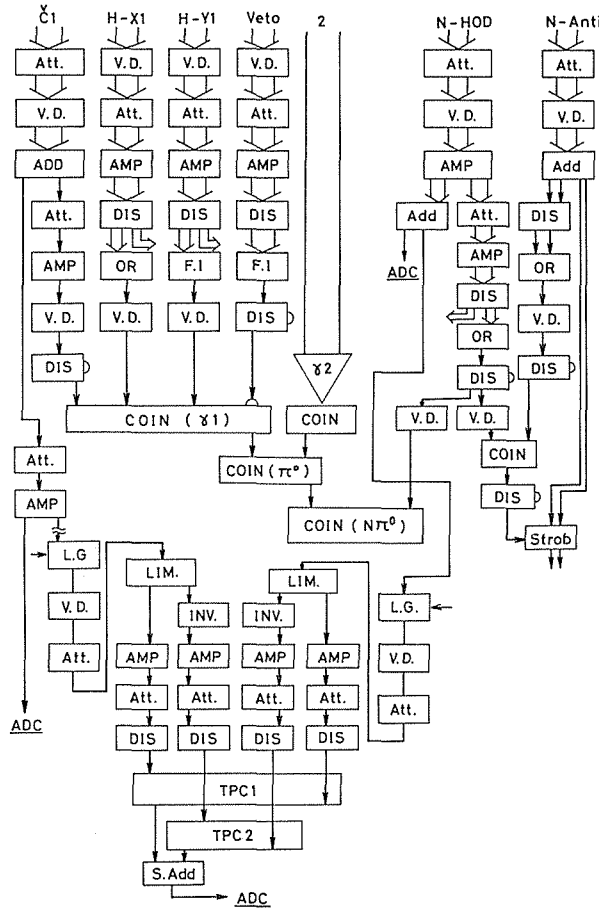

Fig. 6. Block diagram of the electronics. Att.: attenuator; V.D.: variable delay; DIS: discriminator; F.I.: fan-in circuit; ADD: adder; AMP: amplifier; OR: or circuit; COIN: coincidence circuit; L.G.: linear gate; LIM: limitter; INV: inverter; Strob: strobed coincidence circuit; TPC: time to pulse height converter; ADC: analog to digital converter; S. Add.: slow adder.

II-5 Electronics

The block diagram of the electronics is shown in Fig. 6. A photon signal was produced when the coincidence between *C*, *HX*, *HY* and *V* was occured, wheer *C*, *HX*, *HY* and *V* denote the signals from the Cherenkov counter, *x*-, *y*-hodoscope and the veto counter as anti-coincidence, respectively. The π° signal was obtained from the coincidence between two photon signals. The nucleon signal was produced from the nucleon hodoscope and the thin plastic scintillator. Finally the master signal was produced from the coincidence between the π° signal and the nucleon signal.

The on-line data taking system used in the present experiment is shown in Fig. 7. The OKITAC-4300 data processor was placed near the experimental area.

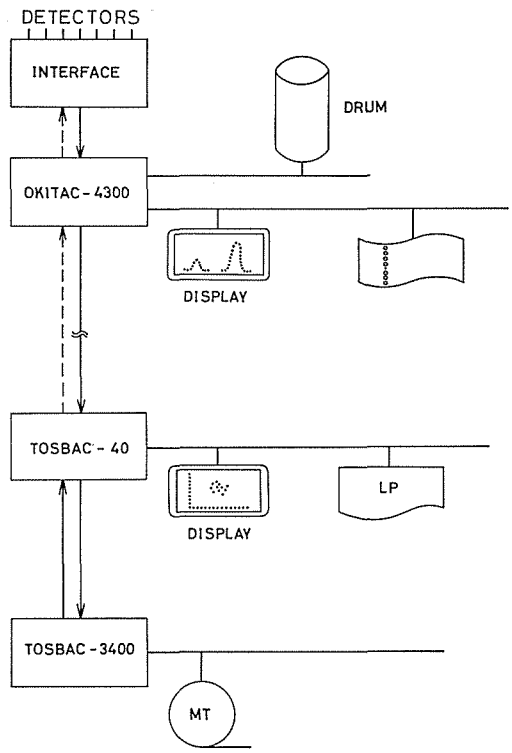

Fig. 7. Block diagram of the on-line system.

This processor was used for storing and monitoring of the raw data. The distribution of the events in the hodoscope, the pulse height distributions of the Cherenkov counter and the nucleon hodoscope and TOF distributions were monitored on the display unit. The stored data were transfered to the central computer at INS, TOSBAC-3400, and were processed. Then the kinematically processed distributions such as of the photon energy and the π° mass were displayed with the TOSBAC-40B processor.

III. Experimental procedure

III-1 Data taking

The set up parameters of the nucleon hodoscope and the π° detector were chosen to have the maximum efficiency under the assumption that the target nucleon was at rest in the laboratory system as in Table I. The distance between the nucleon hodoscope and the target was chosen to be 2–3 m according to the energy of the nucleon to retain good TOF resolutions.

Table I. Setup Parameters

	Cherenkov			Nucleon	
MeV-θ	L_H	θ_π	$\Psi/2$	L_N	θ_N
750–90-D	138.8 cm	63.0°	14.9°	304.4 cm	41.0°
570–90-D	120.8	67.7	18.9	305.0	40.9
420–90-D	110.9	71.1	24.4	304.4	40.9
300–90-D	98.0	71.0	32.5	235.3	41.0
570–110-D	94.4	86.4	21.5	263.0	31.9
450–110-D	100.9	89.7	25.7	263.0	31.9
350–110-D	95.7	91.6	31.2	263.0	31.9
570–130-D	105.3	108.3	24.5	283.8	23.0
450–130-D	105.7	111.6	28.7	283.8	23.0
375–130-D	98.0	113.2	32.5	283.8	23.0
570–70-D	129.9	51.5	16.9	274.7	50.0
420–70-D	117.0	53.7	22.2	274.7	50.0
320–70-D	103.0	52.3	28.3	274.7	50.0
570–90-H	120.9	67.7	18.9	305.0	41.0
420–90-H	121.1	71.1	24.4	305.0	41.0
300–90-H	98.0	71.0	32.5	235.7	41.1

Setup 750–90-D, for example, means that the photon energy in the target at rest system, k_γ^{π}, and the c.m. angle of the π° meson, θ_π^c, are equal to 750 MeV and 90°, respectively, and the target used is liquid deuterium.
L_H and L_N: the distance projected to the horizontal plane between the center of the target and the front surface of the hodoscope of the π° detector and that of the nucleon hodoscope, respectively.
θ_π and θ_N: the angles of the π° detector and the nucleon hodoscope with respect to the direction of the incident bremsstrahlung, respectively.
Ψ: the opening angle of two γ detectors of the π° detector.

When the master signal was produced, the analog informations obtained from both Cherenkov counters, the nucleon hodoscope and TOF, and the digital informations from the x-y and the nucleon hodoscope and the thin plastic sintillator were stored into core memories of the OKITAC-4300 data processor. When 106 events were stored, they were transfered to the drum of 32k words. At the same time they were transferred to the central computer TOSBAC-3400 through the TOSBAC-40B data processor and were processed. At the end of the run, all data were recorded on a magnetic tape of the central computer and were also punched out on a paper tape with the OKITAC-4300 data processor.

The stability of each detector was monitored by counting the single and coincidence rates for every run using scalers and the data processor.

III-2 Address reduction of the hodoscope

The address of the x-y hodoscope of the γ detector coresopnded to 21 $(x)\times$ 5(y) channels, which are divided from 11×3 counters of the overlap type. Because of the lateral spread of showers in the lead converter, adjacent few counters were fired frequently. The maximum number of the fired counters allowed in the address reduction was 4 and 2 for x and y directions, respectively. The address was defined as their center. The channel distributions of the events are shown in Fig. 8. The numbers of events recorded in the overlapped channels were higher than that of the non-overlapped channels due to the shower spread.

Adjacent few counters of the nucleon hodoscope were also fired frequently. The incident position of the nucleon was determined for the events which fired the hodoscope with the same pattern shown in Fig. 9. The multi-fired events rates for

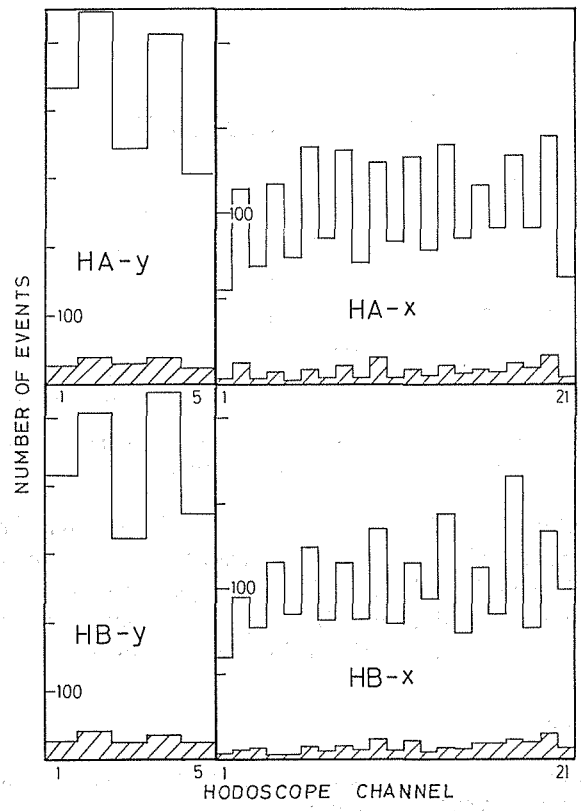

Fig. 8. Event distributions of the Cherenkov hodoscope for the 420 MeV-90°-D setup. The shaded area represents the background.

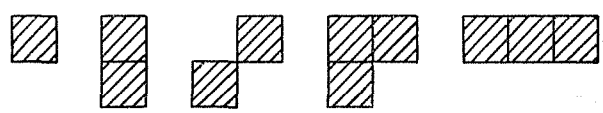

Fig. 9. Patterns of good-fired events of the nucleon hodoscope. The incident position of the nucleon was determined for the events which showed the same patterns as in this figure.

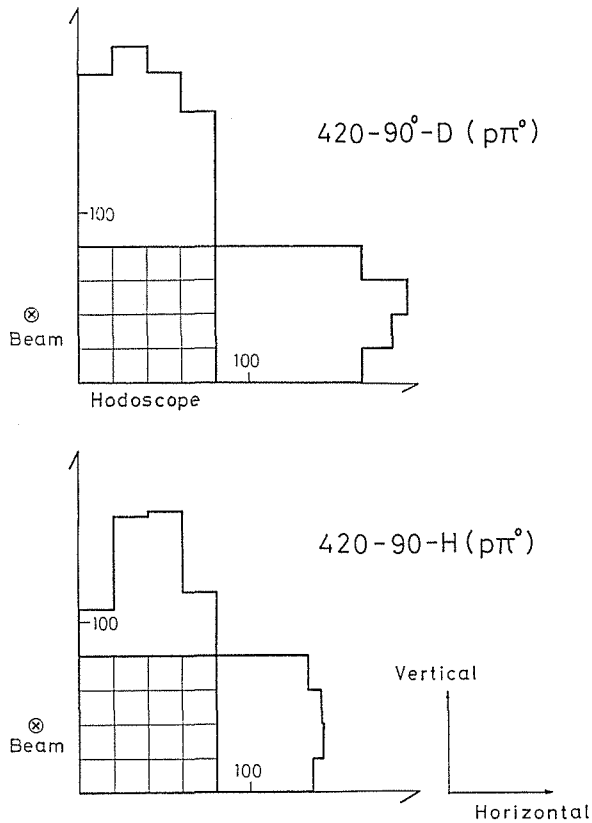

Fig. 10. Event distributions of the neutron hodoscope of the deuterium and the hydrogen target run for the 420 MeV-90° setups.

neutrons and protons were 5–30 % and 5–18 % of the single fired events rates, respectively. A typical distribution of the incident position for protons is shown in Fig. 10. The distribution of the production angle of the proton from the deuterium target is spread over wider angular range than that of the proton from the hydrogen target due to the Fermi motion of the nucleon.

IV. Data reduction

The data stored on the magnetic tape were processed as the following procedure using the TOSBAC-3400 computer.

a) selection of the true events
b) kinematical reconstruction of the events
c) reduction of the ratio R
d) corrections

IV-1 Selection of the true events

The mass of the π° meson, μ, for each event is calculated from the stored data by using the following equation;

$$\mu^2=2k_1\cdot k_2\cdot(1-\cos\Psi)\,, \tag{4-1}$$

where k_1, k_2 are the observed photon energies by the lead glass Cherenkov counters, Ψ is the opening angle between two photons which was reduced from the address of the x-y hodoscope of the γ detector. The mass distribution of the π° meson thus obtained is shown in Fig. 11–b. The events in the low energy tail of the mass distribution were cut off as shown in Fig. 11–b.

The distribution of TOF between the γ detector and the nucleon hodoscope shows a peak. The events under the peak were selected as good events, as is shown in Fig. 11–a. The amount of the accidental coincidence events was estimated from the smooth background distribution at the both sides of the peak in the TOF distribution. The amounts of the background were estimated to be 2–15 % and 8–30 % for the events which correspond to the reactions $\gamma+p\rightarrow\pi^\circ+p$ and $\gamma+n\rightarrow\pi^\circ+n$ for the deuteron target run, respectively.

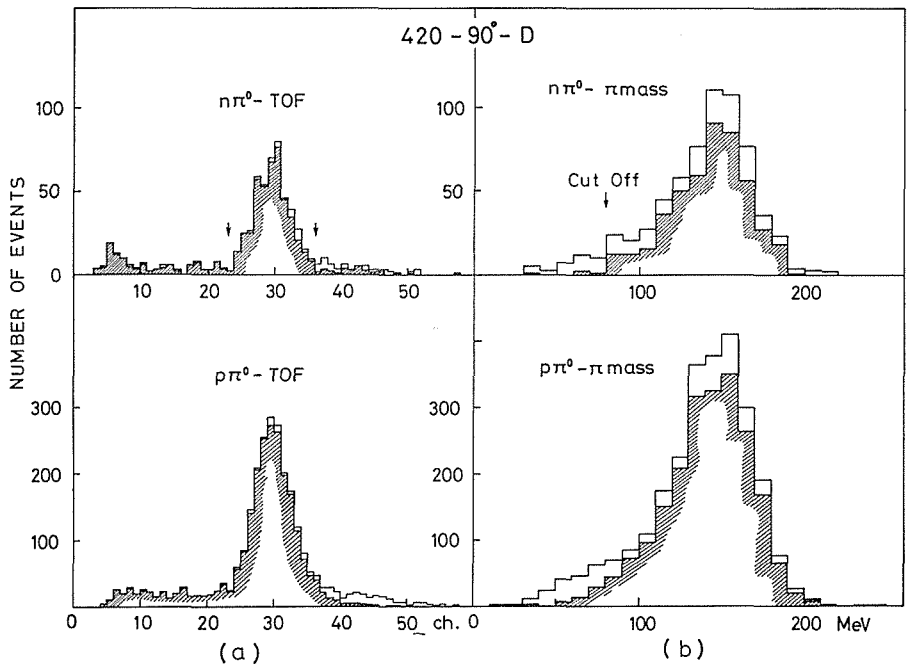

Fig. 11. a) TOF distribution, and b) π° mass distribution calcurated from the equation (4–1) for the 420 MeV-90°-D setup. The upper and lower figures represent the event distributions from the reactions $\gamma+n\rightarrow\pi^\circ+n$ and $\gamma+p\rightarrow\pi^\circ+p$, respectively. The shaded events of the TOF distribution correspond to the events having the π° mass of above the cut off energy. The shaded events of the π° mass distribution correspond to the events lying in the acceptable region of TOF channels.

IV-2 Kinematical reconstruction

The four momentum vector of the π° meson for each event were evaluated from the measured photon energies and decay angles with the following way[14] which is the improvement of Tau's method[15].

Among the measured quantities there should be the following relation;

$$k_1 \cdot k_2 = \frac{\mu^2}{2(1-\cos \Psi)} . \tag{4-2}$$

In the present experiment the accuracy of the measurement on the opening angle Ψ, is better than that of the photon energies k_i. Therefore, the righthand side of the equation (4–2), which is named as A, can be evaluated more accurately than the lefthand side of the equation. The most probable photon energies (k_1', k_2') should be on the hyperbola;

$$k_1' \cdot k_2' = A . \tag{4-3}$$

Assuming that the measured photon energies (k_1, k_2) distribute around the most probable photon energies (k_1', k_2') following the Gaussian distribution, (k_1', k_2') can be obtained by minimizing the following quantity;

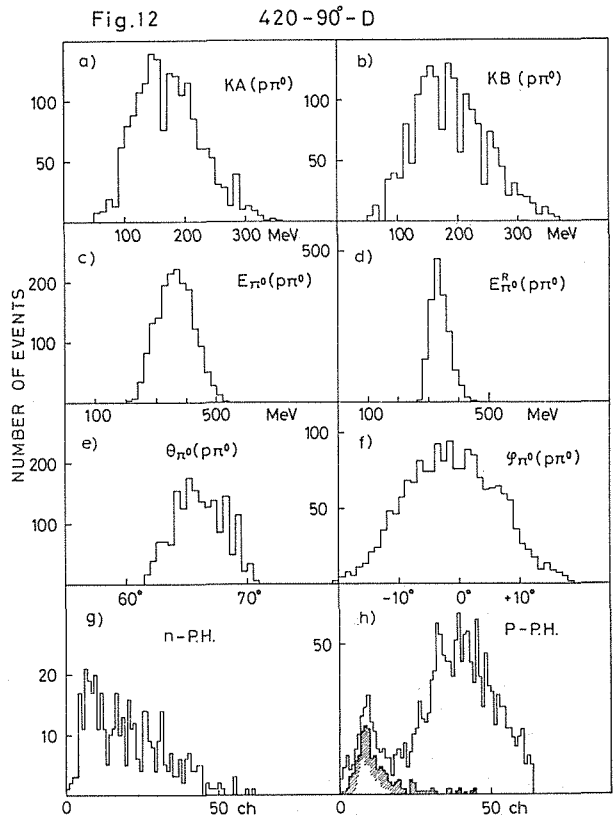

Fig. 12. Event distributions for the 420 MeV-90°-D setup. a), b) pulse heights distributions of a pair of Cherenkov counters. c) the distribution of the energy of the π° meson obtained by adding the energies of two photons; k_A+k_B. d) the distribution of the energy of the π° meson reconstructed by using the method described in section IV–2. e), f) the distributions of the production and azimuthal angles of the π° meson. g), h) the pulse height distributions of the nucleon hodoscope for the neutron and the proton, respectively. The shaded events in the proton distribution shows the background.

$$r^2=\frac{(k_1'-k_1)^2}{(\sigma(k_1'))^2}+\frac{(k_2'-k_2)^2}{(\sigma(k_2'))^2}, \tag{4-4}$$

where $\sigma(k_i')$ denotes the deviation for the photon energy. The deviation for our Chernkov counter is approximated as follows;

$$\sigma(k_i')=c/\sqrt{k_i}, \tag{4-5}$$

where c denotes a constant,
From these equations, (k_1', k_2') is given as follows;

$$k_1'=\sqrt{\frac{A+k_1^2}{A+k_2^2}\cdot A}, \tag{4-6a}$$

$$k_2'=\sqrt{\frac{A+k_2^2}{A+k_1^2}\cdot A}. \tag{4-6b}$$

The most probable photon energies k_1', k_2' were calculated for each event by using above equations. The resolution of the π° energy was estimated to be 3–4 % (FWHM) by the Monte Carlo simulation.

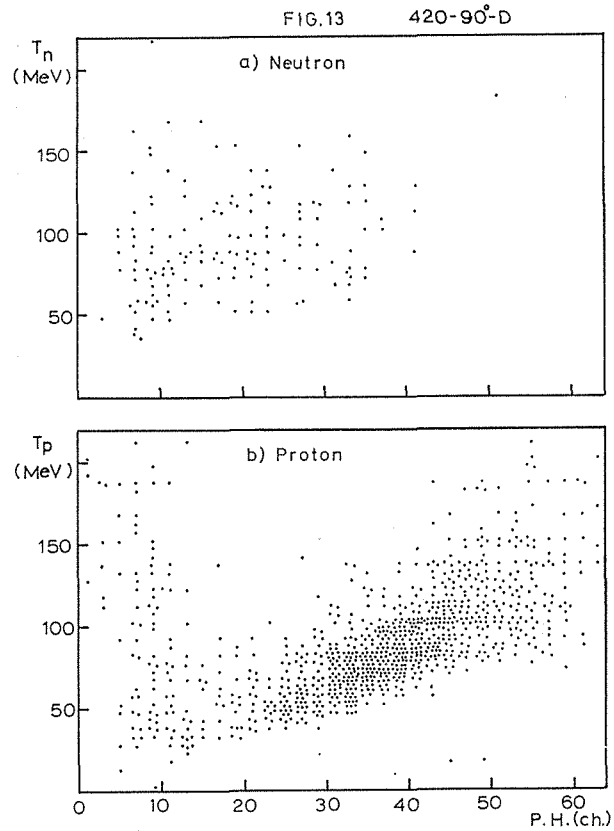

Fig. 13. Correlation between the nucleon kinetic energy and the pulse height of the nucleon hodoscope for a) neutrons and b) protons for the 420 MeV-90°-D setup.

The distributions such as the pulse height of the Cherenkov counter and the energy and the production angle of the π° meson were shown in Fig. 12.

The energy of the nucleon was evaluated from TOF as described previously. The pulse height distributions of the nucleon hodoscope and the correlation between the kinetic energy and the pulse height of the nucleon hodoscope are shown in Fig. 12-g, 12-h and 13, respectively.

Finally, the initial photon energy in the target at rest system, k_γ^R, and the π° c.m. angle, θ_π^c, were obtained by the following equations under the assumption that the target nucleon was free in the deuteron;

$$k_\gamma^R = \frac{1}{m}\left(\omega \cdot E_2 - \boldsymbol{q}\cdot\boldsymbol{P}_2 + \frac{\mu^2}{2}\right), \tag{4-7}$$

$$\cos\theta_\pi^c = \frac{1}{q^c}\left\{(q\cdot\cos\theta_\pi - \omega)\frac{k}{k^c} + \omega^c\right\}, \tag{4-8}$$

where $(\boldsymbol{q}, \omega)$, $(\boldsymbol{P}_2, E_2)$ and $(\boldsymbol{k}, k)$ represent the four momentum vector of the π° meson, the recoil nucleon and the initial photon in the laboratory system, respectively. m and μ represent the rest mass of the nucleon and the π° meson, respectively.

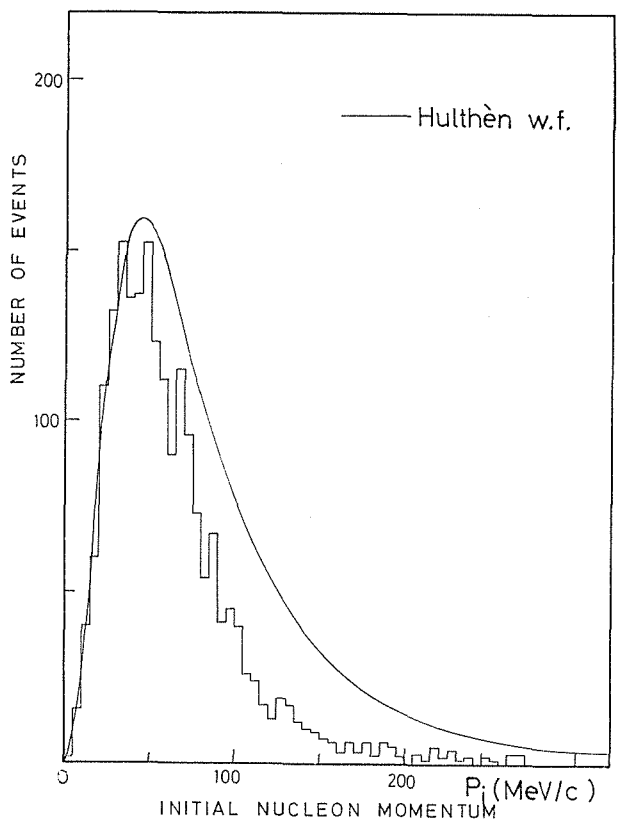

Fig. 14. Momentum distribution of the initial nucleon for the 420 MeV-90°-D setup. The solid curve is the calculated value from the Hulthen wave function.

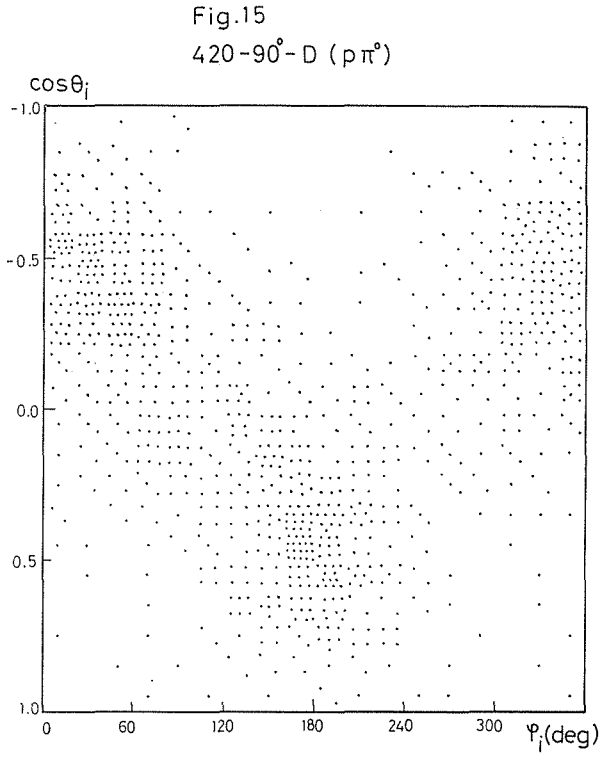

Fig. 15. Directional distribution of the initial nucleon for the 420 MeV-90°-D setup. θ_i and ϕ_i denote the polar and azimuthal angles of the initial nucleon, respectively.

θ_π denotes the production angle of the π° meson in the laboratory system. Variables with a suffix c represent the quantities at the c.m. system.

The momentum, p_i, and the direction, $(\cos\theta_i, \phi_i)$, of the initial target nucleon were also obtained and are shown in Fig. 14 and 15. Since the π° and the nucleon detector were set under the assumption of the two body kinematics in the target at rest system, the higher momentum component of the initial nucleons is detected with a small efficiency when we compared the momentum distribution to that expected from the Hulthen wave function. Also the angular distribution shows that the initial nucleons moving in the two directions were detected with a large efficiency.

IV-3 Reduction of the ratio R

In the present experiment, as the neutron and the proton were detected by the same detectors, the geometrical detection efficiency for both reactions are identical because of the negligibly small mass difference between the neutron and the proton. Taking into account the nucleon detection efficiency in the nucleon hodoscope, the ratio between the experimental yield corresponding to the reaction $\gamma+n\rightarrow\pi^\circ+n$ and $\gamma+p\rightarrow\pi^\circ+p$ can be reduced accurately.

To get the ratio R from the experimental data, it is necessary that the following equation can hold;

$$R=\frac{\frac{d\sigma}{d\Omega}(\gamma+n_{\text{free}}\rightarrow\pi^{\circ}+n)}{\frac{d\sigma}{d\Omega}(\gamma+p_{\text{free}}\rightarrow\pi^{\circ}+p)}=\frac{\frac{d\sigma}{d\Omega}(\gamma+n_{\text{bound}}\rightarrow\pi^{\circ}+n)}{\frac{d\sigma}{d\Omega}(\gamma+p_{\text{bound}}\rightarrow\pi^{\circ}+p)}. \qquad (4\text{-}9)$$

The correction on the cross section due to the Pauli exclusion principle and Coulomb scattering which appear in the charged pion production do not exist for the π° production. However, 'the interference effect' between the spectator nucleon and the target nucleon and the effect due to the multiple scattering might exist. In the π^{-} production measurements with the bubble chamber[7], the interference effect was estimated to be large for the initial nucleon having the high momentum and small for the low momentum, and amounted to be about 5 % in average. Since in the present experiment the initial nucleon having high momentum was detected with the small efficiency as seen in Fig, 14, the interference effect was estimated to be negligibly small.

IV-4 Correction to the data

The background events due to the accidental coincidence were subtracted as discussed in section IV-1. The empty target yield amounted to be less than 12 % and was also subtracted.

A few events which were not rejected by the criterions on the informations of TOF and Cherenkov pulse heights, were rejected because many counters in the x-y hodoscopes of the γ detectors and the nucleon hodoscope were fired. These events were considered to be good events. The errors due to this sort of corrections were 0.6-3 % and 0.4–2 % for the x-y and the nucleon hodoscopes, respectively.

The rate of the accidental coincidence of the veto counters of the γ detectors was estimated to be less than 1 % and was negligibly small.

The detection loss for the low energy protons were appreciable at the runs in the region of the low photon energy and at the forward c.m. angles of the π° meson. The loss amounted to be 8 % and 26 % at the 335 MeV bin at 90° and 335 MeV bin at 70°, respectively.

The background from the double pion production may contribute in the photon energy region above about 450 MeV. Then the top energy of the synchrotron was set about 200 MeV higher than the central energy of the acceptance of the detection system. With this condition the background from the double pion production was estimated to be negligibly small.

V. Results and discussions

V-1 Experimental results

The results on the ratio R were obtained from the data of 13 setups of Table I. The present detection system accepted the events in the rather wide photon energy region of 150 MeV to 400 MeV in width. The energy and angular resolution of our detection system were estimated from the Monte Carlo simulation[16] and amounted to be 20–40 MeV in k_{γ}^{R} and 3–4° in θ_{π}^{c} (FWHM). The events in the tails of the acceptance of k_{γ}^{R} were not included in the final results because of the poor statistics and the inaccuracy of the background subtraction. For each

Table II. Measured values of the ratio R

k_γ^{lab} (MeV)	θ_π^c (deg.)	$R=\pi^\circ n/\pi^\circ p$
335±15	68.0±3.0	1.042±.112
365±15	69.0±4.0	.872±.096
400±20	70.5±2.5	.774±.075
440±20	71.0±3.0	1.016±.100
480±20	73.0±3.0	1.006±.112
530±30	72.0±3.0	1.068±.109
590±30	72.5±2.5	1.163±.144
650±30	73.5±2.5	1.237±.184
710±30	74.0±2.0	1.085±.178
770±30	75.0±2.0	.753±.197
275±15	86.0±2.0	.926±.162
305±15	87.5±2.5	.854±.086
335±15	88.0±3.0	.894±.104
365±15	90.0±3.0	.867±.118
400±20	91.0±3.0	1.066±.105
440±20	90.5±2.5	1.087±.118
480±20	91.5±2.5	1.089±.132
530±30	92.0±3.0	1.074±.123
590±30	91.0±3.0	1.133±.132
650±30	91.0±3.0	1.106±.146
710±30	90.0±3.0	.785±.108
770±30	91.0±3.0	.727±.113
830±30	91.0±2.0	.748±.147
890±30	91.0±2.0	.759±.186
950±30	92.0±2.0	.604±.189
305±15	109.0±3.0	.813±.194
335±15	109.0±3.0	1.215±.145
365±15	109.0±3.0	.970±.092
400±20	109.0±3.0	.933±.074
440±20	110.0±3.0	1.181±.094
480±20	110.0±3.0	1.201±.112
530±30	110.0±3.0	1.403±.131
590±30	109.5±3.5	1.101±.148
650±30	109.0±3.0	1.078±.190
710±30	109.5±2.5	1.250±.280
770±30	110.0±3.0	1.048±.308
335±15	128.0±2.0	.807±.147
365±15	128.5±2.5	.949±.122
400±20	129.0±3.0	1.112±.114
440±20	130.0±3.0	1.181±.140
480±20	130.0±3.0	1.630±.220
530±30	129.5±3.5	1.314±.195
590±30	130.0±3.0	1.556±.314
650±30	129.5±2.5	1.922±.535
710±30	129.5±2.5	1.218±.489
770±30	129.5±2.5	1.399±.576

The symbols k_γ^{lab} and θ_π^c denote the initial photon energy in the target rest system and the c.m. angle of the π° meson, respectively. The errors included are statistical only.

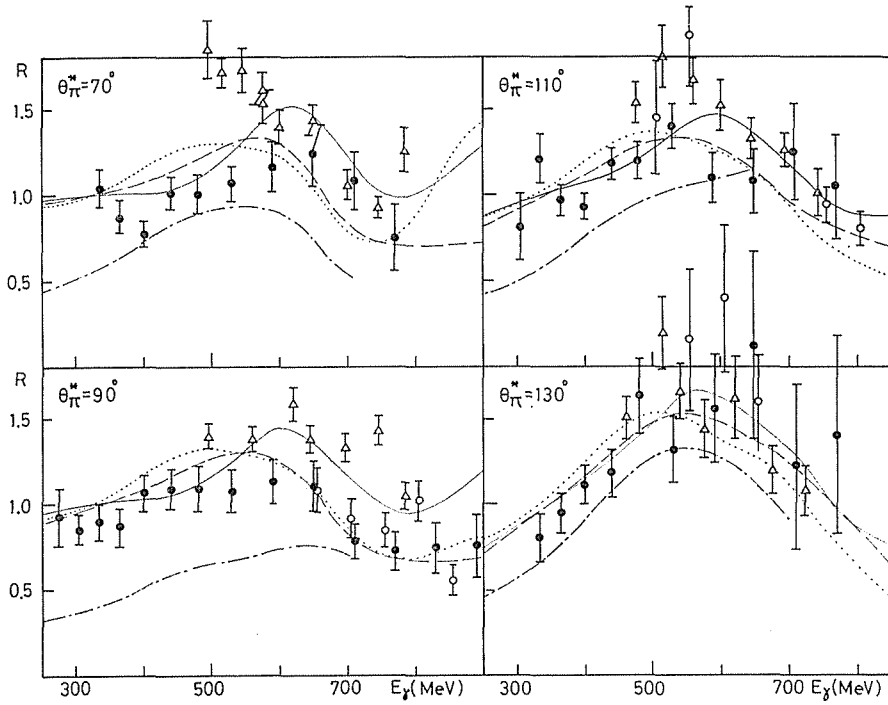

Fig. 16. Results of the ratio $R=[d\sigma/d\Omega(\gamma+n\rightarrow\pi^\circ+n)]/[d\sigma/d\Omega(\gamma+p\rightarrow\pi^\circ+p)]$. The closed circles, open circles and tri-angulars represent the results of the present experiment, Ref. 11 and Ref. 25, respectively. The solid, dashed and dotted curves are calculated using the Walker (Ref. 17), M-O-R (Ref. 19) and M-W (Ref. 18) amplitudes, respectively. The dash-dotted curve is calculated assuming $x=-0.3$ in the equation (5–1) and using the M-W amplitude.

setup, the ratios between the numbers of the event corresponding to the reaction $\gamma+n\rightarrow\pi^\circ+n$ and $\gamma+p\rightarrow\pi^\circ+p$ were evaluated at 4–7 energy intervals which were slightly wider than the energy resolution of the detector.

The ratios which were obtained from different setups and were in the same region of k_γ^R and θ_π^c, were averaged with their weights. The results are tabulated in Table II and shown in Fig. 16.

The present results are consistent with the results at INS[11] within the experimental error, however the results at Frascati[25] at forward angles are higher than the present results. The ratios are about unity arround the $\Delta(1236)$ resonance.

V-2 Discussions

The predictions calculated by using the amplitudes given by Walker[17], Metcalf and Walker (M-W)[18] and Moorhouse *et al.* (M-O-R)[19], are shown in Fig. 16.

In the $\Delta(1236)$ resonance region, the magnetic dipole amplitude, ${}_3M_{1+}$, in the CGLN[21] notation is known to be dominant from phenomenological analyses[22]. Then to investigate the contribution of the isotensor current on the ratio $R=[d\sigma/d\Omega(\gamma+n\rightarrow\pi^\circ+n)]/[d\sigma/d\Omega(\gamma+p\rightarrow\pi^\circ+p)]$, we introduced the parameter x as in Ref. 3 and 10;

$$ {}_3M^n_{1+}=(1+x)\cdot{}_3M^p_{1+}, \tag{5-1}$$

where n and p represent the neutron and proton target respectively. Assuming x to be -0.3 as suggested by recent analyses[3),10)], the ratios were calculated using the amplitude given by M-W analysis and are also shown in Fig. 16. Apparently the ratios decrease to about 0.5 and are not consistent with the present results. The χ^2 fit has been performed on x by using the amplitudes of the M-W analysis. The result is

$$x=-0.065\pm0.072\,, \tag{5-2}$$

with $\chi^2/F=1.02$. The result shows that the isotensor current do not contribute to be $\Delta(1236)$ resonance. The results obtained at Daresbury[23)] and Frascati[24)] are in good agreement with the present result in the energy region of the $\Delta(1236)$ resonance. The amplitudes given by Walker, M-W and M-O-R are not so different each other in the $\Delta(1236)$ resonance region. Therefore, the present result (5-2) obtained by using the amplitude of the M-W analysis is considered to be rather model independent.

In the second resonance region, there are differences on the ratio R between the old analysis by Walker and the recent analyses by M-W and M-O-R, as shown in Fig. 16. In the Walker's analysis, the isoscalar amplitude and the helicity 1/2 amplitude of the $N(1520)$ (D_{13}) resonance are small. In recent analyses, the large isoscalar amplitude which is nearly 20% of the helicity 3/2 part of the $N(1520)$ resonance are used. The amplitude of the helicity 1/2 is about one half of the helicity 3/2 for the neutron target. The above difference is remarkable at 70° and 90° as is shown in Fig. 16. The present results are consistent with the recent analyses. A parameter fitting to the results above 440 MeV was made by varing the resonance peak parameters for A_{2-} B_{2-}, A_{2+}, B_{2+}, A_{3-} and B_{3-} based on the *M-W* analysis without changing the parameter for the $\Delta(1236)$ resonance. The results are tabulated in Table III.

Table III. Resonance Amplitudes

		fit value	M-W[18)]		Walker[17)]	
Res.	W(MeV)	$(\pi^\circ n)$	$(\pi^\circ n)$	$(\pi^\circ p)$	$(\pi^\circ n)$	$(\pi^\circ p)$
A_{2-}	1510	−0.390	−0.371	0.035	−0.001	0.140
B_{2-}	1510	0.807	0.764	1.068	0.820	0.940
A_{2+}	1650	−0.067	−0.014	0.035	——	——
B_{2+}	1650	−0.060	−0.021	−0.100	−0.100	−0.100
A_{3-}	1690	0.041	0.035	0.035	——	——
B_{3-}	1690	0.029	0.000	0.396	0.354	0.425
		(in unit of $(\mu b)^{1/2}$)				

The best fit values were obtained by varing the resonance peak amplitudes corresponding to the reaction $\gamma+n\to\pi^\circ+n$ $(\pi^\circ n)$ with $\chi^2/F=1.88$. The values of M-W and Walker analyses are also presented.

In the $N(1470)$ (P_{11}) resonance region, the ratio R obtained at Frascati[25)] is larger than the present result. They suggested that there is enhancement on the neutron cross section due to the $N(1470)$ resonance. In the present experiment the nucleon and both of two photons decayed from the π° meson were detected. On the otherhand the Frascati group detected the nucleon and only one photon from the π° meson.

The conclusions of the present experiment are summarized as follows. The isotensor amplitude is less than 3 % of the isovector amplitude at the $\Delta(1236)$ resonance. In the second resonance region the result is consistent with the recent phenomenological analyses by M-W and M-O-R. There is no enhancement of the cross section for the reaction $\gamma+n\rightarrow\pi^{\circ}+n$ due to the $N(1470)$ resonance.

Acknowledgment

The auther would like to express his sincere thanks to Prof. K. Miyake and Prof. T. Nakamura for their continuous encouragements and guidances throughout this work. He is deeply grateful to Dr. R. Kikuchi, Dr. Y. Hemmi, Dr. T. Miyachi, Mr. N. Tamura, Mr. Y. Inagaki, Mr. K. Imai, Mr. M. Yoshioka, Mr. A. Ando, Mr. H. Sato, Mr. I. Nakano, Mr. A. Noda and Mr. M. Ono for their advices and collaboration in carrying out this experiment.

Thanks are also due to the members of the electron synchrotron crew under Prof. S. Yamaguchi of the Institute for Nuclear Study for their effort and hospitality in running the synchrotron.

His thanks are also due to the members of the machine shop under Mr. S. Hanazono in constructing the present π° detecting system.

The kinematical computation and the analysis have been performed by the TOSBAC-3400 computer at the Insitute for Nuclear Study.

This work was partially supported by a grant-in-aid for scientific researches of the Ministry of Education.

REFERENCES

1) K. M. Watson; Phys. Rev. **95** (1954) 228.
2) V. G. Grishine, V. L. Lyuboshitz, V. I. Ogievetskii, M. I. Podgoretskii; Sov. J. Nucl. Phys. **4** (1967) 90.
N. Dombey, P. K. Kabir; Phys. Rev. Lett. **17** (1966) 730.
3) A. I. Sanda, G. Shaw; Phys. Rev. Lett. **24** (1970) 1310.
Phys. Rev. **D3** (1971) 243.
4) Aachen - Berlin - Bonn - Hamburg - Heidelberg - Munchen Collaboration; Nucl. Phys. **B8** (1968) 535.
5) Pavia - Rome - Frascati - Napoli Collaboration; Lett. Nuove Cimento **3** (1970) 697.
6) P. A. Berardo, R. P. Haddock, B. M. K. Nefkens, L. J. Verhey, M. E. Zeller, A. S. L. Parsons, P. Truoel; Phys. Rev. Lett. **24** (1970) 419. Phys. Rev. Lett. **26** (1971) 201.
7) Aachen - Bonn - Hamburg - Heidelberg - Munchen Collaboration; DESY 73/19 (1973).
8) T. Fujii, S. Homma, K. Huke, S. Kato, H. Okuno, F. Takasaki, T. Kondo, S. Yamada, I. Endo, H. Fujii; Phys. Rev. Lett. **28** (1972) 1672.
9) G. Von Holtey, G. Knop, H. Stein, J. Stumpfig, H. Wahlen; Phys. Letters **4;B** (1972) 589. PIB 1–209 (1973).
10) A. Donnachie, G. Shaw; Phys. Rev. **D5** (1972) 1117.
11) Y. Hemmi, T. Inagaki, R. Kikuchi, A. Maki, K. Miyake, T. Nakamura, A. Sasaki, N. Tamura, S. Yasumi, H. Okuno; Nucl. Phys. **B55** (1973) 333. Phys. Letters **32B** (1970) 137.
12) Y. Doi, T. Fujii, T. Kitami, H. Okuno, K. Takamatsu; Japan J. Appl. Phys. **10** (1971) 468.
13) Y. Hemmi, R. Kikuchi, S. Kobayashi, K. Miyake, T. Nakamura, H. Okuno, S. Yasumi, Y. Yoshimura; Nucl. Instr. Methods **56** (1967) 213.
14) I. Nakano; Master *thesis* (*in Japanese*).
15) L. Tau; Nucl. Instr. Methods **34** (1965) 352.
16) Y. Inagaki; *private communication.*

17) R. L. Walker; Phys. Rev. **182** (1969) 1729.
18) W. J. Metcalf, R. L. Walker; Calt—68–425 (1974).
19) R. G. Moorhouse, H. Oberlack, A. H. Rosenfeld; Phys. Rev. **D9** (1974) 1.
20) G. Knies, R. G. Moorhouse, H. Oberlack; LBL—2410 (1973).
21) G. F. Chew, M. L. Goldberger, F. E. Low, Y. Nambu; Phys. Rev. **106** (1957) 1395.
22) *see, for example,* Ref. 17.
23) R. W. Clifft, E. Gabathuler, L. S. Littenberg, R. Marshall, S. E. Rock, J. C. Thompson, D. L. Ward, G. R. Brooks; Daresbury *preprint* (1973).
24) E. Di Capua, V. Pocci, M. Severi, L. Tau, E. Fiorentino, F. Palmonari, A. Reale, L. Satta, G. Ubaldini; Lett. Nuovo Cimento **8** (1973) 692.
25) C. Bacci, R. Baldini-Celio, B. Esposito, C. Mencuccini, A. Reale, G. Sciacca, M. Spinetti, A. Zallo; Phys. Letters **39B** (1972) 559.